Journal Pre-proof

Mathematical representation and nonlinear modelling of the Wheatley mitral valve

H.L. Oliveira, G.C. Buscaglia, J.A. Cuminato, S. McKee, I.W. Stewart et al.

PII: S1350-4533(25)00002-5
DOI: https://doi.org/10.1016/j.medengphy.2025.104283
Reference: JJBE 104283

To appear in: *Medical Engineering and Physics*

Received date: 5 January 2024
Revised date: 11 December 2024
Accepted date: 5 January 2025

Highlights

- Analytical formulation of Wheatley surfaces containing two leaflets.
- Proposition of a non-linear model capable of capturing the mechanical behavior of the valve under simplified service conditions.
- Taking non-linear contact forces between leaflets into account for equilibrium stability.
- The results show that the leaflet height does not change the mechanism of force transfer along the valve.

Mathematical representation and nonlinear modelling of the Wheatley mitral valve

H. L. Oliveira[a,b,*], G. C. Buscaglia[b], J. A. Cuminato[b], S. McKee[c], I. W. Stewart[c], M. M. Kerr[d], D. J. Wheatley[e]

[a]*FECFAU - Departamento de Estruturas, Universidade Estadual de Campinas, Cidade Universitária, Av. Albert Einstein, 901, 13083-852, SP, Brazil*
[b]*Instituto de Ciências Matemáticas e de Computação - ICMC, Universidade de São Paulo, Campus de São Carlos, Caixa Postal 668, 13560-970, SP, Brazil*
[c]*Department of Mathematics and Statistics, University of Strathclyde, 26 Richmond St, Glasgow, G1 1XH, United Kingdom*
[d]*Department of Biomedical Engineering, University of Strathclyde, 50 George St, Glasgow, G1 1QE, United Kingdom*
[e]*School of Science and Engineering, University of Dundee, Nethergate, Dundee, DD1 4HN, United Kingdom*

Abstract

This study is concerned with the Wheatley design of the mitral valve. A mathematical description, in terms of elementary functions, is provided for the S-shaped leaflets. This is based on a level set containing symmetric circles (or more generally ellipses) which allow parametrization. A geometric nonlinear mechanical model subjected to a uniform pressure gradient and in the absence of inertial forces is introduced. The model results in a system of nonlinear equations that is solved using iterative incremental techniques. Under normal pressure loads, the S-shaped geometries induce internal forces which manifest themselves in two combined effects: bending and torsion. As a consequence, the supports are subject to periodic bending actions that tend

*Corresponding author
Email address: hugo.oliveira@unicamp.br (H. L. Oliveira)

to deform the support frame towards the interior of the valve. Providing resistance becomes vital for maintaining stable equilibrium. It is also observed that for circular base shape geometries, the mechanism for transmitting the equilibrium forces remains unchanged when the height/diameter ratio is kept below 2.

Keywords: Leaflets analytical description, Finite Element Method, nonlinear analysis, Static structural model

---

1. Introduction

The human heart has a set of four valves that open and close to ensure that blood flows in the correct direction. The four valves are the aortic valve, mitral valve, pulmonary valve and tricuspid valve. Some conditions such as ageing, congenital heart disease, infections, diabetes among others can lead to malfunction of these valves affecting the health of the individual [1]. There are two main types of heart problems that can happen in any of the valves: stenosis, when the valve does not open properly and regurgitation, when the blood flows back due to poor valve closure. Diseases associated with the aortic valve account for 61% of deaths from heart valve disease, while diseases associated with the mitral valve account for 15%, with regurgitation being one of the most prevalent occurrences [2].

In general, valve pathologies can be divided into two classes: primary (or degenerative), when the disease is related to the valve itself, and secondary, when the disease results from dysfunction of adjacent cardiac structures. In the case of mitral regurgitation, primary causes are leaflet prolapse or chordal rupture, and secondary causes are ischaemic heart disease or cardiomyopathy

[3]. When the mitral valve functions poorly and there is no possibility of surgical repair, then valve replacement becomes a treatment option [4].

There are two main types of replacement mitral valves: tissue valves and mechanical valves. Tissue valves, also called biological or bioprosthetic valves, are made from animal tissue. In general, tissue valves wear out with time and require new medical interventions. On the other hand, mechanical valves are made from durable materials and generally do not wear out. However, patients will need to take anticoagulants for life [5, 6]. As a consequence, the development of replacement valves that are both durable and minimise the impact on the patient's life is of prime importance, and remains an active field of research [7, 8].

In terms of valve replacement design, numerous studies have demonstrated the benefits that numerical and computer simulations can provide, e.g. [9]. The formulations allow complex behaviours such as durability, biological response and haemodynamics to be investigated in a single model. From an engineering point of view, an ideal valve should not only cause reduced pressure drops, but also ensure minimal regurgitation volume, minimise turbulence production, avoid zones of high shear stresses and flow stagnation [10]. In addition, the designer should avoid valve shapes that lead to low washout performance since this is a coagulation-facilitating factor [11, 12, 13, 14].

Substantial work has been done by Wheatley et al. [15] on the function of experimental polymeric valves of conventional design. Intending to create a design that not only preserves the good features of existing prosthetic heart valves, but also potentially improves the washout effect, D. J. Wheatley introduced the concept of S-shaped leaflets [16, 17, 18]. The geometry of the leaflets can be obtained from the union of circular and elliptical contour lines so that a family of shapes becomes readily obtainable, which is of crucial importance for manufacturing processes [19, 20]. From these geometries, computational models can be built to simulate the global behaviour of the assembly [21]. Approaches such as these have been increasingly applied in the design of state-of-the-art valves [22, 23, 24]. In the present study we investigate Wheatley's design for bi-leaflet mitral valves.

The contribution of this study is twofold. We first present a formulation describing the leaflet surface inspired by Wheatley's design with a view to mitral prosthetic valve applications. Although the defining parameters are different, it is essentially a natural extension of previous work on the Wheatley aortic valve where we introduced mathematical representations of the Wheatley valve using elementary functions [19, 20, 21]. Secondly, we present a geometric nonlinear structural model capable of predicting the behaviour of the leaflets in the absence of inertial forces under uniform pressure gradients.

Producing a mathematical representation of the design is a useful first step before applying computational fluid dynamics to understand both the blood flow in the valve and the cavities (atrium, ventricle), and the internal leaflet stresses during valve function. Of course, the shape could have been generated via splines, but the principal advantage of a mathematical representation with elementary functions is that it permits shape changes to be easily trialled. For instance, the three-dimensional shape can be obtained directly by making linear increments along the z direction. However, this is not the only option; quadratic, cubic or higher order increments and even transcendental functions are also possible in an analytical approach. That creates a family of designs, providing a flexibility that is not available with the use of splines.

2. Numerical Modelling

2.1. Wheatley geometric design

In this section we present a closed mathematical representation of the Wheatley Mitral Valve.

2.1.1. The artificial mitral valve

A paper version of the mitral valve is displayed in Figure 1. From this, we are able to deduce the contour lines (set of points where a given scalar function assumes a constant value - see Figure 2). Indeed, close inspection of the paper valve and its associated contour lines suggests that, for each contour line, there exists four underlying symmetrically placed circles. These are displayed in Figure 3; the great circle is, for convenience, and without any loss of generality, the unit circle.

2.1.2. Generalization from circles to ellipses

In this section we shall, nonetheless, replace the circles with ellipses: not only is this more general providing an infinite number of designs, it also allows us to obtain the original Wheatley design as a special case. Thus, in place of Figure 3, consider Figure 4 and the two ellipses, CHB, CFD lying on the axis $y = 0$. Let their major axes be $2a$ and $2(1-a)$ (so that their foci are a and $1-a$), respectively. Furthermore, let them both pass through $x = 1$.

Figure 1: Paper model of the Wheatley mitral valve.

Their equations can readily be found to be :

$$\frac{(x-(1-a))^2}{a^2}+\frac{y^2}{(\gamma a)^2} = 1, \quad (1)$$

$$\frac{(x-a)^2}{(1-a)^2}+\frac{y^2}{(\gamma(1-a))^2} = 1, \quad (2)$$

where γ is a measure of 'ellipticity' and is related to the common eccen-

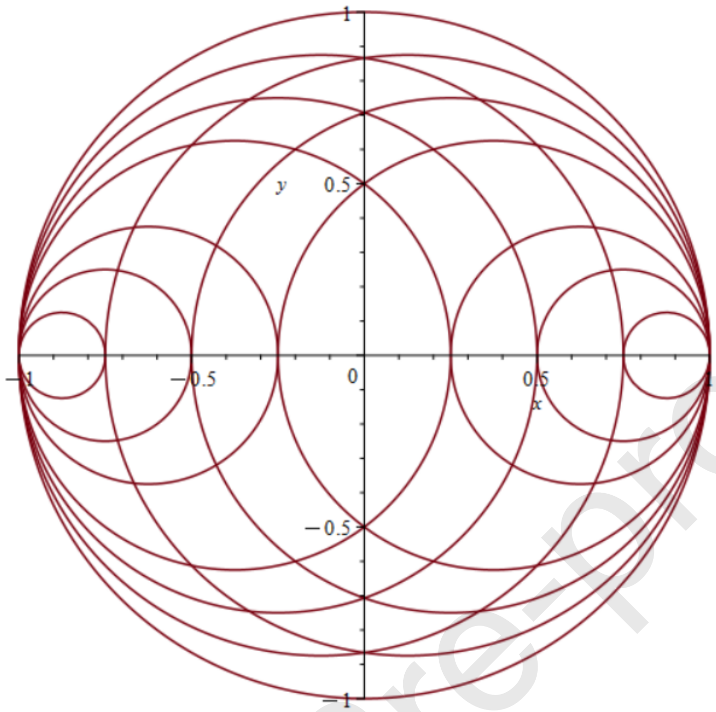

Figure 2: Mitral valve contour lines.

tricity, e, of the two ellipses:

$$\gamma^2 = 1 - e^2.$$

To obtain the equations of the two ellipses AGD and AEB it is only necessary to rotate (1) and (2) by π radians. We therefore immediately obtain

$$\frac{(x+(1-a))^2}{a^2} + \frac{y^2}{(\gamma a)^2} = 1, \tag{3}$$
$$\frac{(x+a)^2}{(1-a)^2} + \frac{y^2}{(\gamma(1-a))^2} = 1. \tag{4}$$

The choice of $\gamma = 1$ reduces the above equations (1) ...(4) to those of

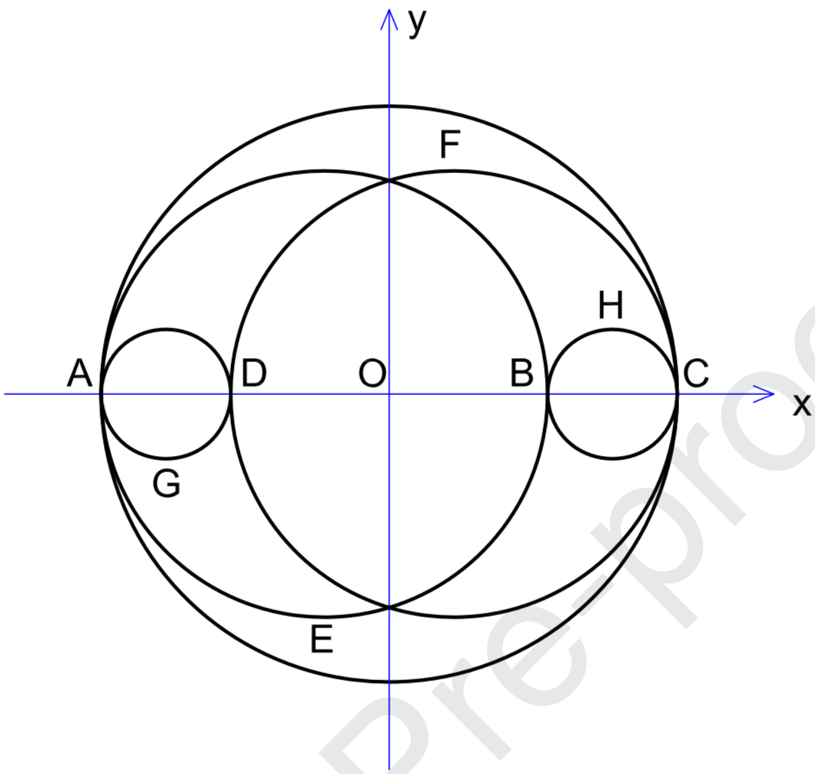

Figure 3: Two large and two smaller circles with the auxiliary unit circle.

circles shown in Figure 3.

2.1.3. Parametrization of the elliptic equations

For graphical purposes we require a parametrization of the four ellipses. Note we wish to trace the arcs CHBEA and AGDFC (red lines in Figure 4). We may write the four equations (1), (2), (3) and (4) in parametrized form as

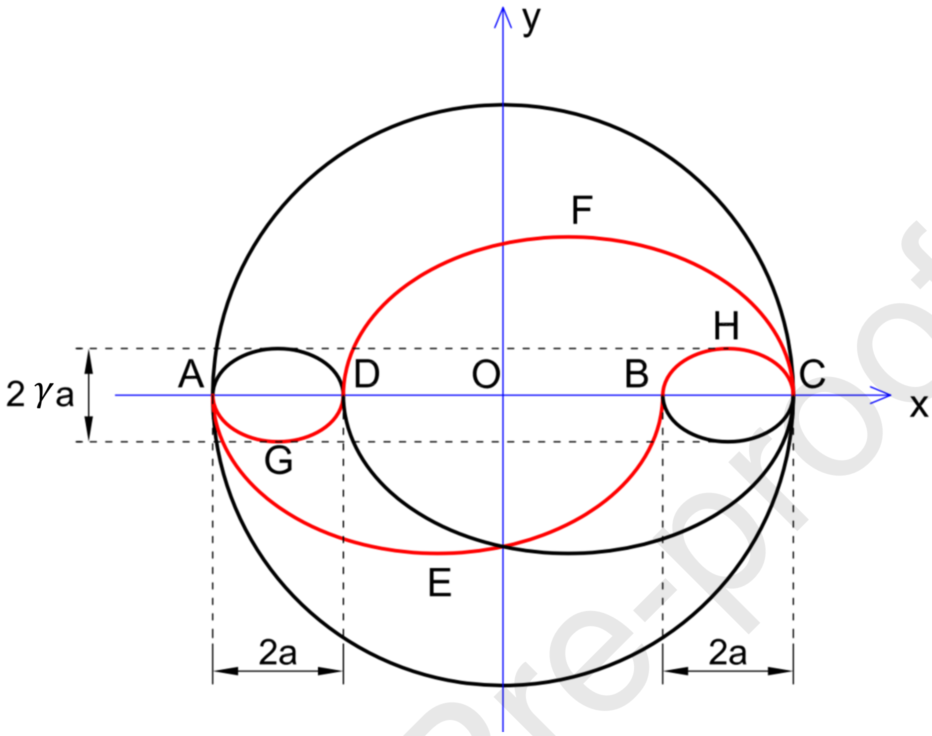

Figure 4: One large circle and four ellipses.

$$
\begin{aligned}
x &= 1 - a + a\cos(\theta),\ y = \gamma a \sin(\theta), & (5)\\
x &= a + (1-a)\cos(\theta),\ y = \gamma(1-a)\sin(\theta), & (6)\\
x &= -(1-a) + a\cos(\theta),\ y = \gamma a \sin(\theta), & (7)\\
x &= -a + (1-a)\cos(\theta),\ y = \gamma(1-a)\sin(\theta). & (8)
\end{aligned}
$$

Recall that we wish to trace out certain arcs: the arc CHB and the arc BEA, and the arc AGD and the arc DFC. In order to do this we require both starting and end points. These are the following: for (5) we need θ to range from 0 to π; for (6) we require θ to go from π to 2π; for (7) we need θ run from 0 to $-\pi$; and for (8) we must have θ ranging from 0 to π.

2.1.4. Examples of the Wheatley elliptic mitral valve

In this subsection we display examples of the geometrical representation of the generalized Wheatley mitral valve, for $\gamma = 1$ (Figure 5a) and $\gamma = \frac{1}{2}$ (Figure 5b). In the special case when $\gamma = 1$ (the original Wheatley valve) the ellipses reduce to circles. In this case the valve is displayed partially open (Figure 5c) and closed (Figure 5d).

The equations that describe the three-dimensional shape of the leaflets allow opening and closing to be performed. Although these motions are kinematically compatible, they do not preserve linear and angular momentum, nor do they follow material-specific responses. To be consistent with the first principles of mechanics, it is necessary to design a geometric nonlinear model, which will be detailed in the next subsection.

2.2. Computational mesh

In this step we establish a finite element mesh that describes the geometry of interest. The original circular design ($\gamma = 1$) is chosen. The dimensions assumed are: $20\,mm$ diameter at the base, $10\,mm$ high. At the top of the leaflets there are two semi-circles of $5\,mm$ radius. The mesh (Figure 6) contains 19321 linear interpolation shell (SHELL181) elements (quadrilateral, triangles), $200\,\mu m$ element size and 19452 nodes. Each node has 6 degrees of freedom (three translations and three rotations). Both leaflets have a uniform thickness of $250\,\mu m$.

2.3. Material response

In the present study, St Venant-Kirchhoff hyperelastic material is assumed. Its relevance lies not only in its simplicity, but also by serving as a

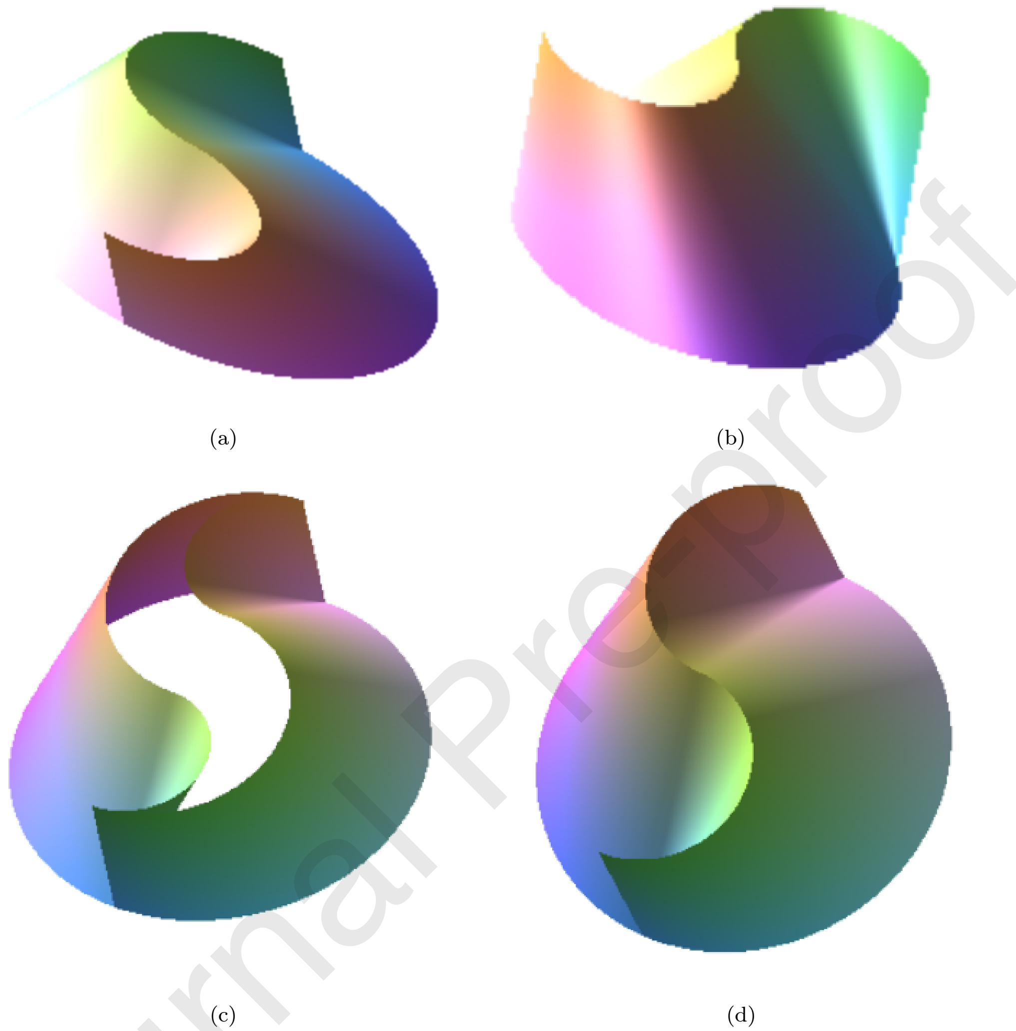

Figure 5: Mitral valve for (a) $\gamma = 2$, (b) $\gamma = 1/2$ (c) $\gamma = 1$ (open) (d) $\gamma = 1$ (closed).

gateway to more elaborate material models. The resulting elasticity matrix has the same form as the linear elasticity formulation, except that Green-Lagrange strains are used. The second Piola-Kirchhoff stress tensor ($\mathbf{S}$) is symmetric and is related to the Green-Lagrange strain tensor ($\mathbf{E}$) according

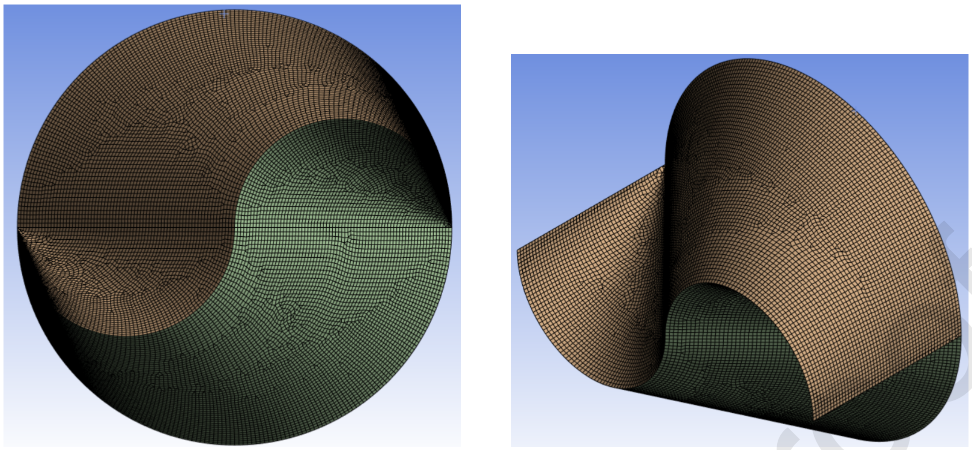

(a) (b)

Figure 6: Finite element mesh in the reference configuration: (a) Top view and (b) Perspective view. (116.712 degrees of freedom)

to the St. Venant constitutive expression:

$$\mathbf{S} = \lambda \mathrm{tr}(\mathbf{E})\mathbf{I} + 2\mu\mathbf{E}, \tag{9}$$

where λ and μ are material parameters known as Lamé constants, and $\mathbf{I}$ is the second order unit tensor. The quantities λ and μ are related to the usual Young Modulus (E) and Poisson ratio (ν) as follows:

$$\lambda = \frac{E\nu}{(1+\nu)(1-2\nu)}, \tag{10}$$

$$\mu = \frac{E}{2(1+\nu)}. \tag{11}$$

The values employed in the model are shown in Table 1. It corresponds to a thermoplastic polyurethane (TPU), although the definitive Wheatley Valve material has not yet been established. The motivation for these parameters came from a previous study carried out by our group, which is described in reference [24].

It is worth noting that this formulation takes into account both the potential initial stresses and the change of configuration due to large displacements.

Table 1: Input parameters for the mechanical models

Parameter	Description	Value
ν	Poisson's ratio	0.49
E	Young modulus	65 MPa

2.4. Boundary conditions

When the valve is positioned between the atrial and ventricular cavities, the movement of the leaflets is induced by the pressure gradient exerted by the blood. In this study, this condition will be approximated assuming that the valve motion will be caused by a normal pressure evenly distributed along the surface following the variation shown in Figure 7. The base of the valve (which is annular) and the vertical posts are kept fixed throughout the stress analysis.

2.5. Contact conditions

Contact modelling is crucial for predicting the functioning of the valve. In biomedical community, the contact region between the two fully closed leaflets is known as the coaptation surface. In pre-transplant patients, this surface distributes the mechanical forces between the two leaflets and the commissural regions of the valve. Proper coaptation modelling is important

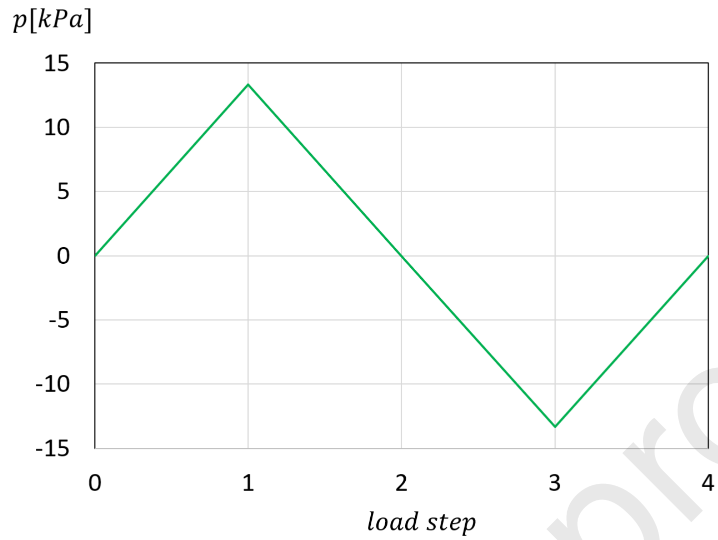

Figure 7: Normal pressure load curve.

not only to obtain force distributions in agreement with first mechanical principles but also to capture physiological haemodynamics.

As both surfaces are flexible, it makes no difference which leaflet will be set as the *target*. We assume that the surfaces in contact can transmit shear forces in addition to compressive forces. When the equivalent shear stress is less than a limit frictional stress (τ_{lim}), no motion occurs between the two surfaces. This state is known as sticking. Once the equivalent frictional stress exceeds τ_{lim}, both surfaces will slide relative to each other. This condition is known as sliding. When cohesion is assumed, sliding resistance exists even in the absence of normal surface pressures. The transition point between sticking and sliding is calculated according to Coulomb's Law:

$$\tau_{lim} = \alpha p + \beta, \tag{12}$$

$$||\tau|| = \sqrt{\tau_1^2 + \tau_2^2} \leq \tau_{lim}. \tag{13}$$

where τ_1 and τ_2 are frictional components in direction 1 and 2 (mutually perpendicular) defined on the contact surface, α is the friction coefficient, p is the contact normal pressure and β is the contact cohesion.

It is also possible to define the maximum equivalent frictional stress τ_{lim} so that, regardless of the magnitude of the contact pressure, sliding will occur if the magnitude of the equivalent frictional stress reaches this value [25]. Figure 8 displays a graphical representation of the frictional model.

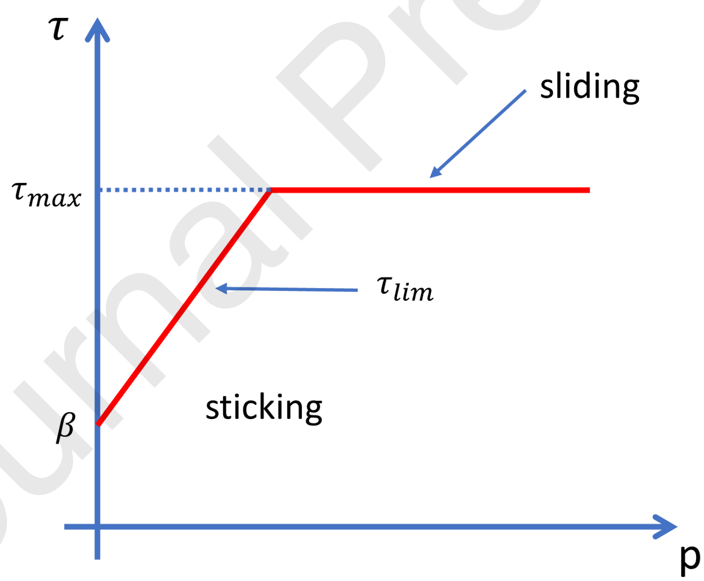

Figure 8: Graphic representation of the friction model.

2.6. Computational Structural Mechanics

The general dynamical analysis of the mitral leaflets gives rise to the equation [26, 27]:

$$[\mathbb{M}]\{\ddot{U}\} + [\mathbb{C}]\{\dot{U}\} + [\mathbb{K}]\{U\} = \{F\}, \tag{14}$$

where $\{U\}$ is the displacement, while $\{\ddot{U}\}$ and $\{\dot{U}\}$ represent the displacements' first and second derivatives, $[\mathbb{M}]$ is the mass matrix, $[\mathbb{C}]$ and $[\mathbb{K}]$ are the material damping and stiffness matrices, respectively, and $\{F\}$ represents the total forces, internal and external, acting on the mitral leaflets. In this study, we assume that inertial and damping forces can be neglected.

The finite element mesh (Section 2.2) is used to build a displacement field ($\{u\}$) approximated by polynomial shape function ($[\mathbb{H}]$ in matrix form), $\{u\} = [\mathbb{H}]\{U\}$. Following Sung and Kwak [28], taking into account the contact forces, equation (14) can be linearized fo provide $\Delta\{U\}$, which reads as follows:

$$([\mathbb{K}_L] + [\mathbb{K}_{NL}])\Delta\{U\} = \{F\}_{ext}^{\mathrm{t}+\Delta\mathrm{t}} - \{F\}_{int}^{\mathrm{t}} + \{F\}_{c}^{\mathrm{t}+\Delta\mathrm{t}}, \tag{15}$$

where

$$\{F\}_{ext}^{\mathrm{t+\Delta t}} = \mathbf{A} \int_{\Omega_{0_e}} [\mathbb{H}]^\top \{b\} \; \mathrm{d}\Omega + \mathbf{A} \int_{\partial\Omega_{0_e}} [\mathbb{H}]^\top \{P\}_0 \; \mathrm{d}\partial\Omega, \tag{16}$$

$$\{F\}_{int}^{\mathrm{t}} = \mathbf{A} \int_{\Omega_{0_e}} [\mathbb{B}_L]^\top [\mathbf{S}]^{\mathrm{t}} \; \mathrm{d}\Omega, \tag{17}$$

$$\{F\}_{c}^{\mathrm{t+\Delta t}} = \mathbf{A} \int_{\Gamma_{0_e}^c} [\mathbb{H}]^\top (p\{\mathbf{n}\} + \tau\{\mathbf{m}\}) \mathrm{d}\Gamma_0^c, \tag{18}$$

$$[\mathbb{K}_L] = \mathbf{A} \int_{\Omega_{0_e}} [\mathbb{B}_L]^\top [\mathbb{D}][\mathbb{B}_L] \; \mathrm{d}\Omega, \tag{19}$$

$$[\mathbb{K}_{NL}] = \mathbf{A} \int_{\Omega_{0_e}} [\mathbb{B}_{NL}]^\top [\mathbb{S}][\mathbb{B}_{NL}] \; \mathrm{d}\Omega. \tag{20}$$

In these expressions, the superscript '$\top$' denotes the transpose operation, 't' and '$t + \Delta t$' represents the previous and current time step and subindex 'e' indicates a given element. $\mathbf{A}$ denotes the standard assembling operator over all elements in the mesh, $\{b\}$ is the body force and $\{P\}_0$ the surface traction. Ω_{0_e} is a given element and $\Gamma_{0_e}^c$ is the potential contact surfaces, both at the reference configuration. $[\mathbb{B}_L]$ is a matrix that depends on the shape function derivatives and that converts the nodal displacements to the linear part of the strains. Similarly, $[\mathbb{B}_{NL}]$ depends on the shape function derivatives and relates the nodal displacements to the nonlinear portion of the strains. $[\mathbb{D}]$ represents the material stiffness matrix and $[\mathbb{S}]$ stores the second Piola-Kirchhoff components in diagonal blocks. $\mathbf{n}$ and $\mathbf{m}$ are normal and tangential directions defined locally in each element.

2.7. Solution Technique

The solution at each time step is obtained via an incremental iterative scheme using (15). Starting from a known solution ($\{U\}^n$), an increment

$\Delta\{U\} = \{U\}^{n+1} - \{U\}^n$ is sought so that the residual forces ($\{R\}$) are zero, that is:

$$\{R\} = \{F\}_{ext}^{\mathrm{t+\Delta t}} - \{F\}_{int}^{\mathrm{t}} + \{F\}_{c}^{\mathrm{t+\Delta t}} = 0. \tag{21}$$

Since several sources of nonlinearity are present in the model, the residual rarely vanishes after the first iteration. This gives rise to unbalanced forces from the previous iteration (k) which are used to calculate nodal displacement corrections, so that:

$$([\mathbb{K}_L] + [\mathbb{K}_{NL}])^k \Delta\{U\}^{k+1} = \{R\}^k. \tag{22}$$

Iterations continue until the residual becomes negligible to within a specified tolerance. In this situation the converged nodal displacement $\{U\}^{n+1}$ is obtained by adding all the corrections:

$$\{U\}^{n+1} = \{U\} + \Delta\{U\}, \tag{23}$$

$$\Delta\{U\} = \sum_{k=1}^{NT} \Delta\{U\}^k, \tag{24}$$

where NT denotes the total number of iterations required for convergence. This process belongs to the class of Newton-based methods. In the present study, the computational model was implemented using Ansys Mechanical APDL 2021R2 solver.

3. Results and Discussion

3.1. Opening and Closing mechanism

Figure 9 shows the colour map representing the magnitude of the displacements observed both at opening and closing. The peculiar shape of the leaflets makes the closing mechanism essentially composed of two global responses: bending and torsion. Bending occurs in each of the leaflets so that the regions which are farthest from the supports have greater movement. The displacement amplitude shown by the free surfaces determines the degree of opening of the valve (nearly 4 mm or half the nominal valve height). Torsion, on the other hand, appears as a joint effect promoted by contact and which leads to rotation of the upper circular boundaries near the valve axis. The maximum displacements in the vertical downward direction is close to 30% of the nominal height.

The effects related to displacements are also observed in the stress field, as shown in Figure 10. Although Von Mises stresses are used to predict yielding in metallic materials, they also serve as a global analysis parameter because they can represent a single scalar measure of the stress state. The colour map in Figure 10 indicates the path of the internal stresses that maintain equilibrium in both the open and closed position. The stresses are not distributed regularly, but instead tend to follow the regions with greater vertical and horizontal stiffness (near the supports and contacts). There is stress concentration in the joint region between the valve base and the vertical supports, as expected, since it is a geometric singularity point. Points such as these may require special attention in studies involving fatigue endurance.

Note that the imposed pressure load does not allow the full opening of

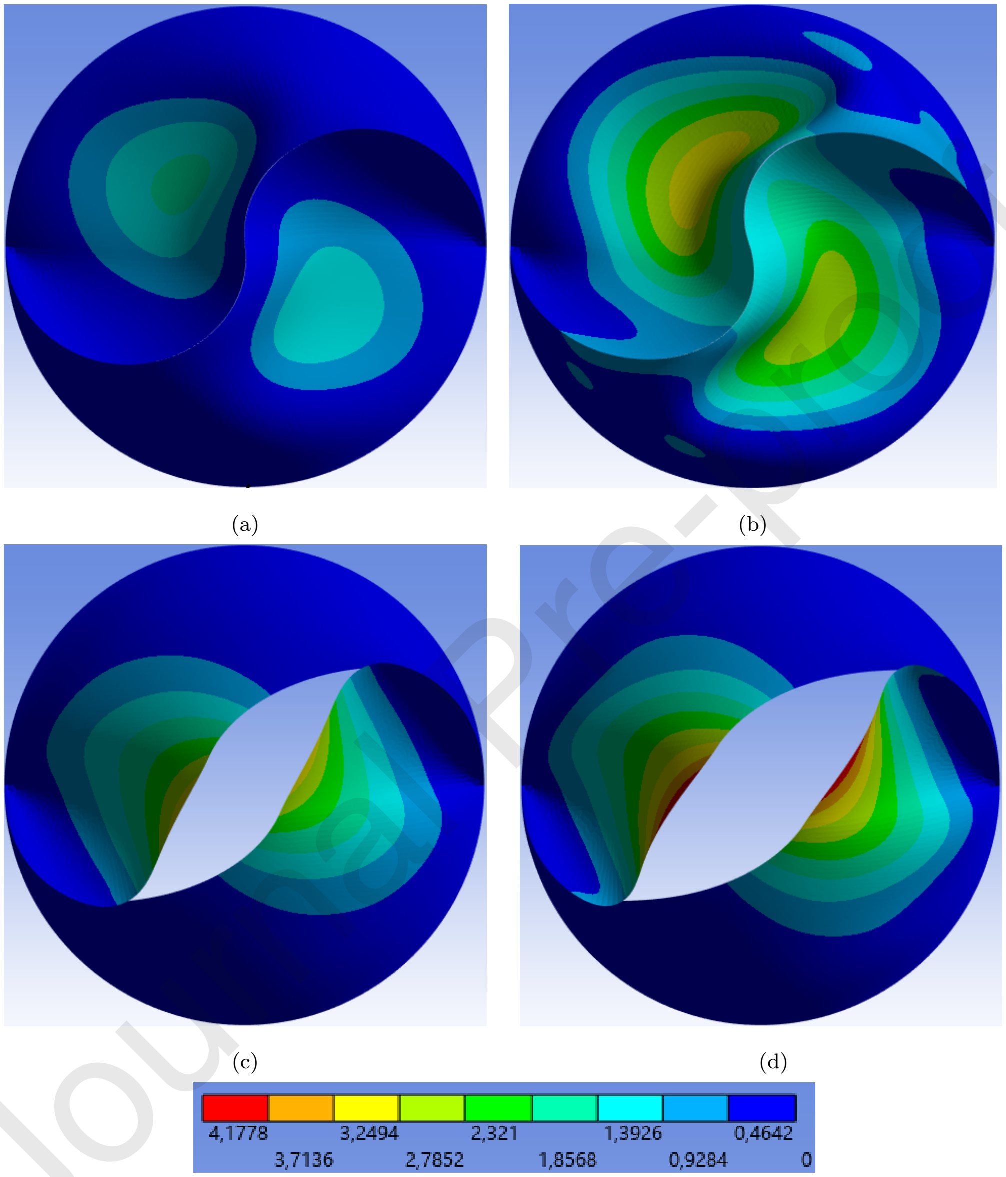

Figure 9: Global displacement field: (a) $step = 0.5$, (b) $step = 1.0$, (c) $step = 2.5$ and (d) $step = 3.0$. Units in mm.

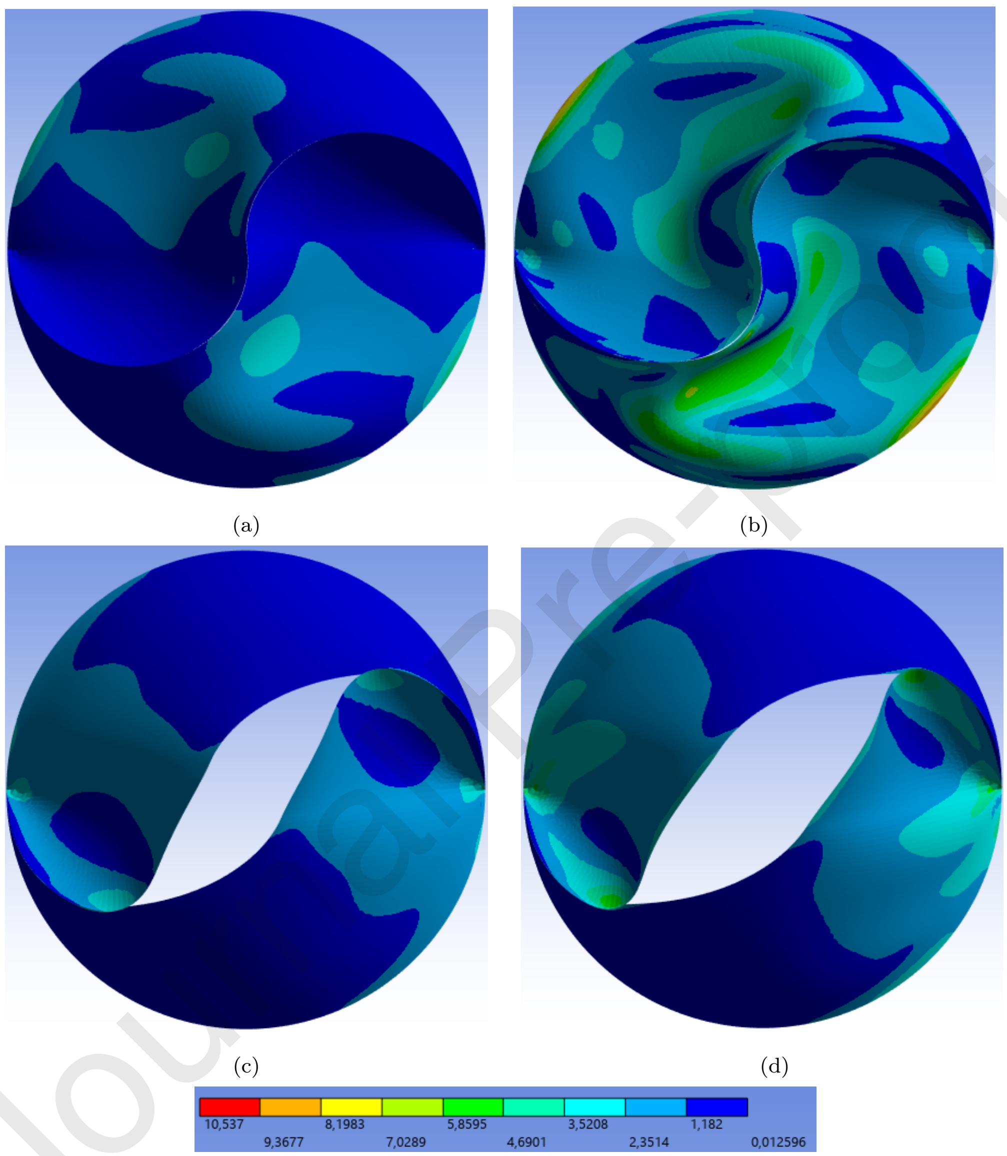

Figure 10: Von Mises stress field: (a) $step = 0.5$, (b) $step = 1.0$, (c) $step = 2.5$ and (d) $step = 3.0$. Units in MPa.

the leaflets. The area of the circular base is 3.14 cm^2. In the position of maximum opening, the minimum orifice area is 0.34 cm^2, or approximately 11%. Naturally this opening rate can be changed by appropriate choice of materials and manufacturing thickness of the leaflets.

3.2. Distribution of bearing forces

An important aspect in any valve concept is to design supports capable of upholding the loads that will act on it, including the possibility of changing the modulus, direction and sense of the support reactions. This structural behaviour can be estimated based on the force fields distribution along the surfaces, in particular, near regions of discontinuity such as contacts and connections.

The way the forces are distributed along the annulus, as well as its proper geometric positioning can have an impact on the efficiency of the valve's operation. For instance, recent studies using in silico modelling have demonstrated that annuloplasticity (for natural mitral valves) with moderate annular reduction may be efficient for achieving optimal coaptation, compared with traditional annuloplasticity techniques [29].

To illustrate the internal force field, Figure 11 displays the fields for two key step loads (1.0 and 3.0). These forces are derived from elemental data (such as stresses and strains) calculated at integration points and then extrapolated to the nodes. The arrows indicate the direction of the acting forces, and their sizes are in proportion. As can be seen, there is a concentration of forces on the contact surface which acts by mobilising the valve opening and closing mechanisms. These forces are responsible for maintaining balance together with the forces on the support frame, represented by the annular base and the vertical supports.

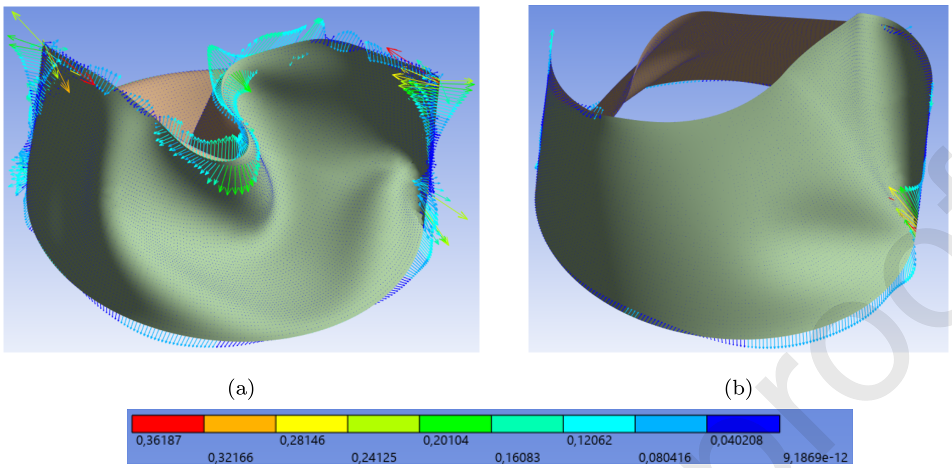

Figure 11: Internal vector force field: (a)$step = 1.0$ and (b) $step = 3.0$. Units in Newtons.

In Figure 12, the same force field is shown restricted to the support regions, adding transparency on the leaflet surfaces. This field of reaction vectors confirms the existence of concentrated forces at the junction between the valve base and the vertical supports (discussed in the Section 3.1). The forces on both the circular base and the vertical supports induce bending. For vertical ones the forces tend to bend the supports towards the interior of the valve, while the base tends to bend in an alternating direction, either inwards or outwards from the circle. As the forces lie in planes not necessarily parallel to the shell surfaces, this indicates that the assumptions associated with shell kinematics are preferable to those for membranes, at least for this application.

These results illustrate that the supporting structure of the leaflets must be sufficiently resistant to bending forces in multiple directions for equilibrium to be preserved. In general the frames are made of rigid material, but

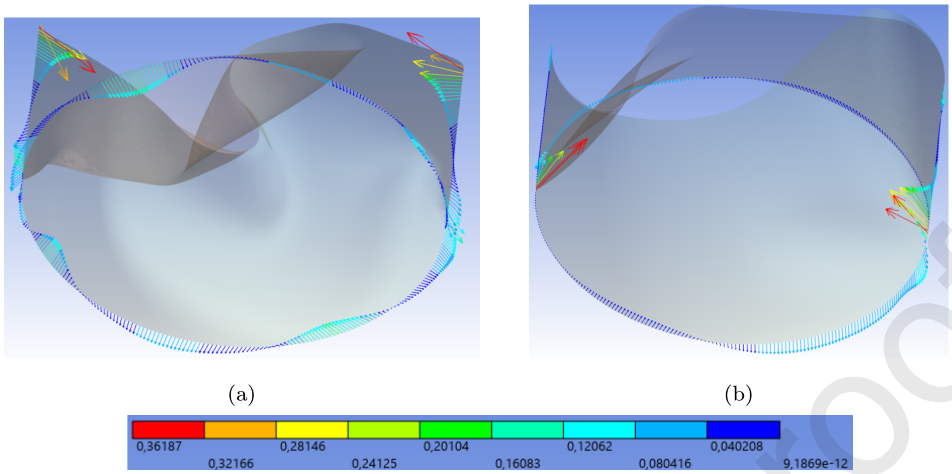

Figure 12: Internal force field along the supports: (a)$step = 1.0$ and (b) $step = 3.0$. Units in Newtons.

the possibility of more flexible structures is not excluded.

3.3. Effect of height for global stability

Three geometries with different heights (10 mm, 15 mm, and 20 mm) were analysed. The other model parameters such as ellipticity degree, constitutive model, contact assumptions, pressure loading curve, characteristic mesh size and kinematic boundary conditions were kept unchanged.

Table 2 shows a comparison between results for three designs. It can be seen that the pattern of both leaflet opening and closing mechanisms remains unchanged with increasing height/diameter ratio. The most notable difference consists of the amplitude of displacements of the free surface at the upper edge, which naturally tends to move further downwards. It is also observed that the free hole of the opening (top view) increases with increasing height of the valve. This gain in flexibility in the upper part can be explained by the transfer of forces from the lower supports to the upright ones, leaving

	$h/d = 0.5$	$h/d = 0.75$	$h/d = 1.0$
Side View	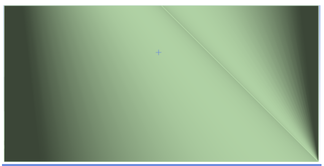	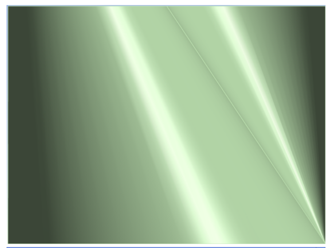	
Deformation (Max closed position)	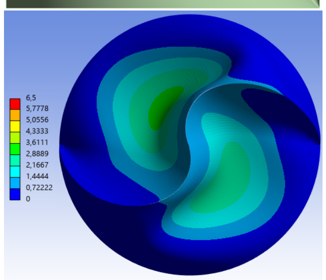	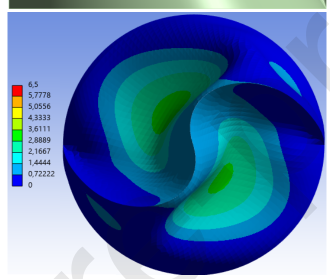	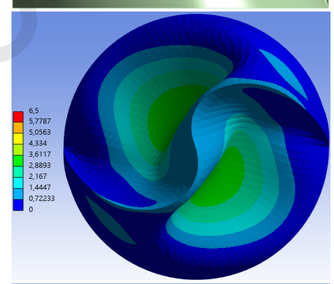
Deformation (Max opened position)	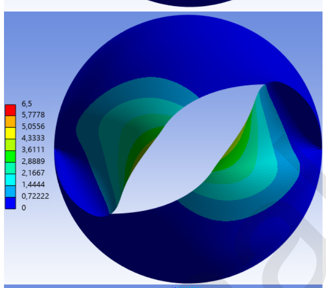	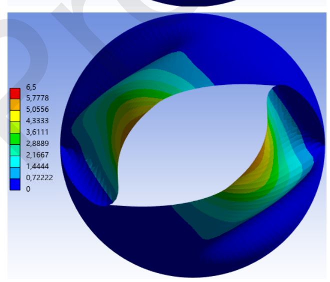	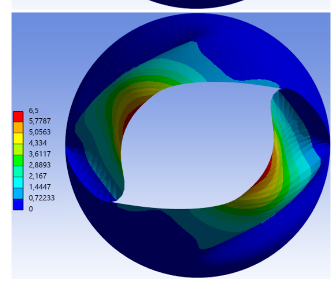
Reaction forces (Max closed position)	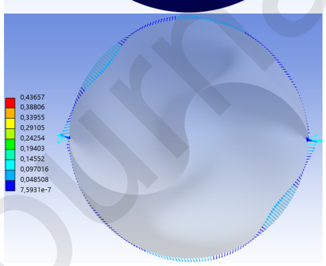	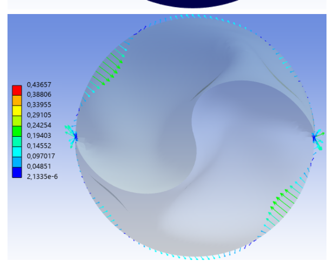	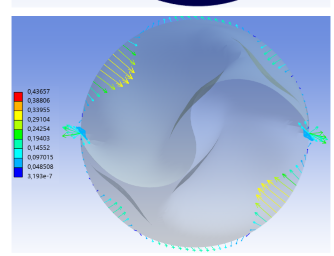
Von Mises Stress (Max closed position)	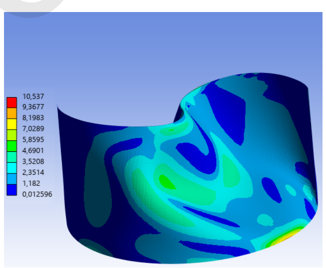	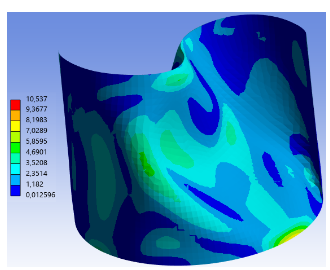	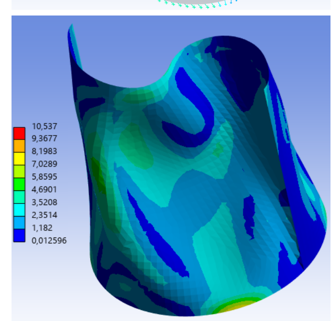

Table 2: Maximum opening and closing positions considering three height (h) to diameter (d) ratios. In all cases the ellipticity degree is $\gamma = 1$. (Units in millimetres, reaction forces in Newtons, Stresses in MPa).

the surface less strained when opening. The alternating bending forces on the supports are maintained, but with different intensities, decreasing as the height increases.

3.4. Comparing S-shaped and U-shape design

Since the formulation proposed in this study is used to design S-shaped valves, it is interesting to compare the mechanical behaviour between the proposed leaflets and the traditional design (chosen here as the U-shaped). In this numerical experiment, both valves (Figure 13) have the same characteristic lengths, same boundary conditions and are simulated using the same constitutive material (Table 1). The contour plots representing mechanical indicators are showed in Table 3.

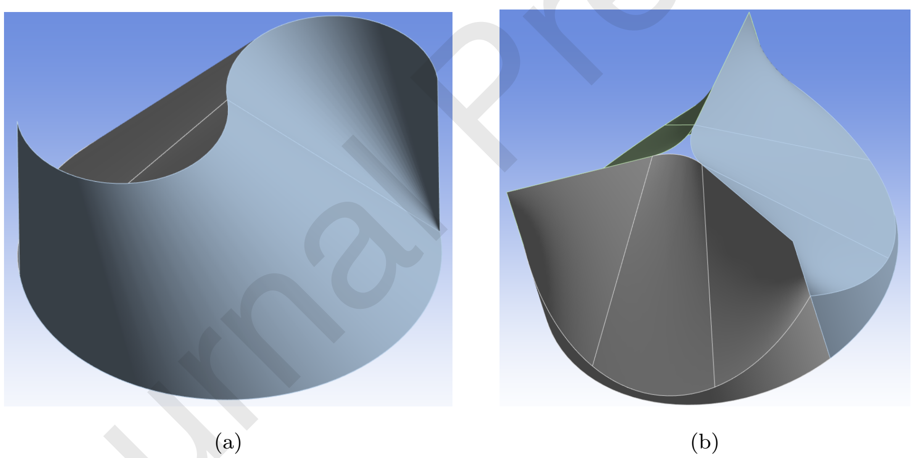

Figure 13: Perspective view of compared designs: (a) S-shape-based and (b) U-shape-based valves. In both cases, annular diameter = 20 mm, height = 10 mm, thickness of leaflets = 250 μm are assumed.

In terms of global displacements, the S-shape design shows higher magnitudes compared to the U-shape. This effect is due to the larger portion of material placed near the centre of the valve that can be moved vertically. This implies that for small pressure increments large displacements occur before tensile stresses can be mobilised to increase geometric rigidity. This arrangement contrasts with the U-shape. In mechanical terms, the U-shape is more stiff with respect to the forces that tend to close the valve.

Regarding the stress distribution, as expected, there is a concentration near the bottom of the vertical posts in the case of the S-shaped valve, which does not occur for the U-shape. This is due to the folding effect of the leaflets on themselves, which tends to create high local stresses. In open position, the S shape creates relatively comparative low stress regions, which provides the possibility for geometric optimisation in future designs.

These results show that the U-shaped valve is uniformly stressed in terms of bending, tensile and geometric stiffness. This doesn't leave much room for improvement on these surfaces. In the case of the S-shape, regions of high stress and regions of low stress can be seen, which may suggest that there exist more convenient curvatures to be used. This type of study could be carried out using parametric analyses and the equations presented here are very attractive for iterative search algorithms.

It is worth noting that the higher geometric stiffness of the S shape implies that the valve has a smaller central opening. This behaviour can induce flow direction as long as the leaflets can withstand the bending stresses. This characteristic can be exploited for specific purposes, in particular for irregular cavities to optimize the outflow volume. In this case, more in depth studies involving fluid-structure interaction are indicated.

<table>
<tr><th></th><th>S-shape</th><th>U-shape</th></tr>
<tr><td>Deformation
(Max closed position)</td><td>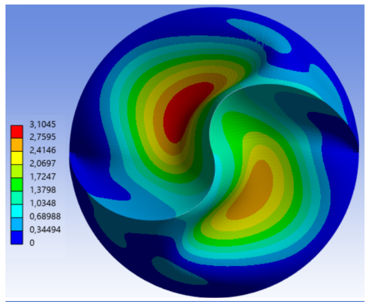</td><td>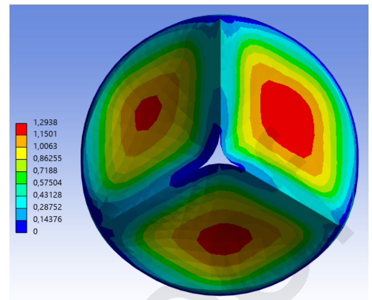</td></tr>
<tr><td>Deformation
(Max opened position)</td><td>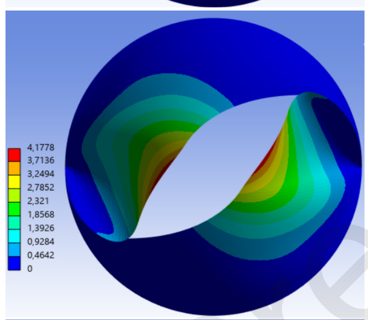</td><td>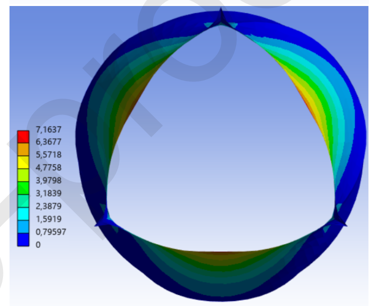</td></tr>
<tr><td>Von Mises Stress
(Max closed position)</td><td>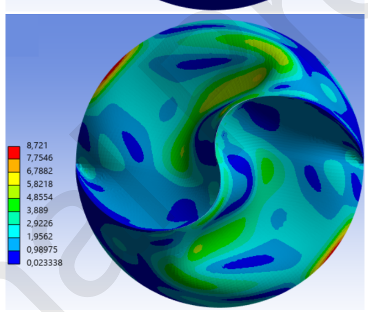</td><td>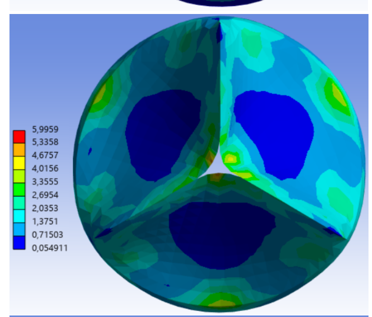</td></tr>
<tr><td>Von Mises Stress
(Max opened position)</td><td>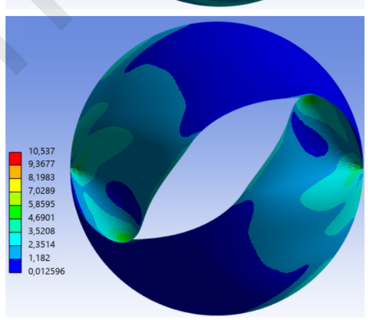</td><td>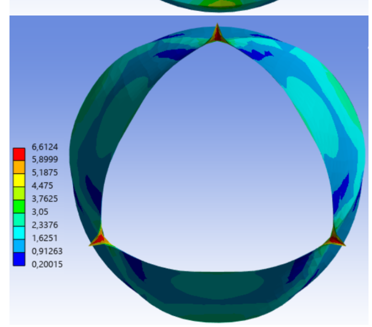</td></tr>
</table>

Table 3: Results for S- and U- shape designs. For S-shape, the ellipticity degree is $\gamma = 1$. (Maximum opening and closing positions units in millimetres, Stresses in MPa).

4. Conclusion

In this work, based on the Wheatley concept, we presented a mathematical description of the leaflets of mitral valves and a nonlinear model of their movement. This procedure has been shown to be efficient for the mechanical performance study of a class of S-shaped leaflet designs. Some points are worth highlighting.

Regarding the purely geometric aspects, it can be remarked that:

(i) This is a natural development from previous work on the Wheatley aortic valve ([19], [20] and [21]). We have taken this further by using ellipses to produce infinitely many designs controlled by a factor γ, which essentially measures the degree of ellipticity in the design;

(ii) Two examples of the closed valve have been displayed for different 'ellipticities'. In addition the original Wheatley valve is shown both closed and partially open. Although these motions are kinematically admissible, they do not follow the equilibrium and material compatibility. However, these equations serve for both analysis and manufacturing design. Hence their importance.

Concerning the nonlinear structural model, it can be observed that:

(iii) It was designed to predict the behaviour of a valve obtained from the equations assuming $\gamma = 1$. However the same procedure remains valid for different degrees of ellipticity;

(iv) The essential aspects of this model are: linear behaviour between Green's deformations and the Second Piola-Kirchhoff Tensor, disregard of inertial forces, consideration of large displacements, uniform pressure gradients on the surface and contact between leaflets. These aspects are considered to be the minimum necessary to capture the opening and closing motions. Changes in these assumptions necessarily imply an adaptation of the model presented here;

(v) The S-shape of the leaflets induces internal forces that mobilise two global responses: bending and torsion. These two effects depends on the contact between the flexible surfaces and upon the stiffness of the support;

(vi) The supports here have been considered completely rigid. In this situation, to maintain the valve equilibrium, the supports are subjected to forces in alternate directions. If flexible bearing frames were adopted these effects should be carefully considered in order to avoid structural instabilities.

(vii) The mechanism for transmitting the equilibrium forces does not change when the height is increased (but not more than double) while maintaining the base diameter.

With regard to the numerical experiment comparing an S-shaped valve with a U-shaped valve:

(viii) The simulation showed that S-shaped leaflets have higher levels of bending, particularly in the central portion of the valve, when compared to U-shaped leaflets. However, this displacement does not hinder the closing mechanism, which remains stable and able to bear the required pressure.

In general, both the method used and the model proposed can be extended to study the Wheatley mitral valve in different scenarios.

Competing interests

The authors declare that David J. Wheatley is the inventor of the valve which was the subject of this study, holding patents in several countries including US Patent No. 9259313 2014, UK Patent No. EP2982340 2016, Europe Patent No. EP2979666 2016 and China Patent No. CN103384505. The full list is available at https://www.wheatleyresearch.co.uk/blog/development-history.

Funding

Grant 2021/11129-0, São Paulo Research Foundation (FAPESP).

Ethical approval

Not required.

References

[1] J. E. Hall and M. E. Hall. *Guyton and Hall textbook of medical physiology.* Elsevier Health Sciences, Philadelphia, PA, 14th edition, 2020.

[2] J. S. Aluru, A. Barsouk, K. Saginala, P. Rawla, and A. Barsouk. Valvular heart disease epidemiology. *Medical Sciences*, 10(32):1 – 12, 2022.

[3] S. Coffey, R. Roberts-Thomson, A. Brown, J. Carapetis, M. Chen, M. Enriquez-Sarano, L. Zühlke, and B. D. Prendergast. Global epidemiology of valvular heart disease. *Nature Reviews Cardiology*, 18(12):853–864, 2021.

[4] R. A. E. Ramsingh, G. D. Angelini, R. D. Rampersad, N. C. Rahaman, and G. Teodori. Early-and long-term outcomes of mitral valve repair in a low-volume centre in the caribbean. *Brazilian Journal of Cardiovascular Surgery*, 37:207–211, 2021.

[5] M. N. Tillquist and T. M. Maddox. Cardiac crossroads: deciding between mechanical or bioprosthetic heart valve replacement. *Patient Prefer Adherence*, 5(1):91–99, 2011.

[6] C. Harris, B. Croce, and C. Cao. Tissue and mechanical heart valves. *Annals of cardiothoracic surgery*, 4(4):399, 2015.

[7] S. H. Gharaie and Y. Morsi. A novel design of a polymeric aortic valve. *The International journal of artificial organs*, 38(5):259–270, 2015.

[8] P. Tschorn, F. Schröter, M. Hartrumpf, R. Kühnel, R. Ostovar, and J. M. Albes. Engineering a new polymeric heart valve using 3d printing - triskelion. *Medicina*, 58(11):1695–1705, 2022.

[9] S. S. Abbas, M. S. Nasif, and R. Al-Waked. State-of-the-art numerical fluid–structure interaction methods for aortic and mitral heart valves simulations: A review. *Simulation*, 98(1):3–34, 2022.

[10] A. P. Yoganathan, Z. He, and S. Casey Jones. Fluid mechanics of heart valves. *Annual review of biomedical engineering*, 6(1):331–362, 2004.

[11] G. D. Dangas, J. I. Weitz, G. Giustino, R. Makkar, and R. Mehran. Prosthetic heart valve thrombosis. *Journal of the American College of Cardiology*, 68(24):2670–2689, 2016.

[12] M. M. Samyn and J. F. LaDisa. Novel applications of cardiovascular magnetic resonance imaging-based computational fluid dynamics modeling in pediatric cardiovascular and congenital heart disease. In *Assessment of cellular and organ function and dysfunction using direct and derived MRI methodologies*. IntechOpen, 2016.

[13] P. H. Zhang, C. Tkatch, R. Newman, W. Grimme, D. Vainchtein, and J. Y. Kresh. The mechanics of spiral flow: Enhanced washout and transport. *Artificial Organs*, 43(12):1144–1153, 2019.

[14] P. H. Zhang, C. Tkatch, D. Vainchtein, and J. Y. Kresh. Aortic hemodynamics of spiral-flow-generated mechanical assistance. *The Annals of Thoracic Surgery*, 109(5):1449–1457, 2020.

[15] D. J. Wheatley, G. M. Bernacca, M. M. Tolland, B. O'connor, J. Fisher, and D. F. Williams. Hydrodynamic function of a biostable polyurethane flexible heart valve after six months in sheep. *The International journal of artificial organs*, 24(2):95–101, 2001.

[16] D. J. Wheatley. Heart valve. *US Patent 9259313*, 2014.

[17] D. J. Wheatley. Heart valve. *UK Patent EP2982340*, 2016.

[18] D. J. Wheatley. Heart valve. *European Patent EP2979666*, 2016.

[19] S. McKee, J. A. Cuminato, I. W. Stewart, and D. J. Wheatley. A mathematical representation of the wheatley heart valve. *Journal of Biomechanical Engineering*, 143(8):1 – 6, 2021.

[20] R. J. Rebolledo, S. McKee, J. A. Cuminato, I. W. Stewart, and D. J. Wheatley. Regularization of a mathematical model of the wheatley heart valve. *Journal of Biomechanical Engineering*, 145(1):1 – 3, 2022.

[21] H. L. Oliveira, S. McKee, G. C. Buscaglia, J. A. Cuminato, I. W. Stewart, and D. J. Wheatley. A generalized mathematical representation of the shape of the wheatley heart valve and the associated static stress fields upon opening and closing. *IMA Journal of Applied Mathematics*, 87(4):537–567, 2022.

[22] L. Cai, R. Zhang, Y. Li, G. Zhu, X. Ma, Y. Wang, X. Luo, and H. Gao. The comparison of different constitutive laws and fiber architectures for the aortic valve on fluid–structure interaction simulation. *Frontiers in Physiology*, 12:1 – 17, 2021.

[23] N. W. Bressloff. Leaflet stresses during full device simulation of crimping to 6 mm in transcatheter aortic valve implantation, tavi. *Cardiovascular Engineering and Technology*, 13:735–750, 2022.

[24] H. L. Oliveira, G. C. Buscaglia, R. R. Paz, F. Del Pin, J. A. Cuminato, M. Kerr, S. McKee, I. W. Stewart, and D. J. Wheatley. Three-dimensional fluid-structure interaction simulation of the wheatley aortic valve. *International journal for numerical methods in biomedical engineering*, page e3792, 2023.

[25] Ansys Inc. Theory reference for the mechanical APDL and mechanical applications. 2021.

[26] R. De Borst, M. A. Crisfield, J. J. C. Remmers, and C. V. Verhoosel. *Nonlinear finite element analysis of solids and structures*. John Wiley & Sons, 2012.

[27] O. C. Zienkiewicz and R. L. Taylor. *The finite element method: solid mechanics*, volume 2. Butterworth-heinemann, 5th edition, 2000.

[28] J. H. Sung and B. M. Kwak. Large displacement dynamic analysis with frictional contact by linear complementarity formulation. *Computers & structures*, 80(11):977–988, 2002.

[29] Hans Martin Aguilera, Robert Matongo Persson, Rune Haaverstad, Bjørn Skallerud, Victorien Prot, and Stig Urheim. In silico analysis provides insights for patient-specific annuloplasty in barlow's disease. *JTCVS open*, 13:95–105, 2023.

Journal: MEDICAL ENGINEERING & PHYSICS

Title of Paper: Mathematical representation and nonlinear modelling of the Wheatley mitral valve

Declarations

The following additional information is required for submission. Please note that this form runs over two pages and failure to respond to these questions/statements will mean your submission will be returned to you. **If you have nothing to declare in any of these categories then this should be stated.**

Conflict of interest
All authors must disclose any financial and personal relationships with other people or organisations that could inappropriately influence (bias) their work. Examples of potential conflicts of interest include employment, consultancies, stock ownership, honoraria, paid expert testimony, patent applications/registrations, and grants or other funding.

Conflicts of Interest

The authors declare that David J. Wheatley is the inventor of the valve which was the subject of this study, holding patents in several countries including US Patent No. 9259313 2014, UK Patent No. EP2982340 2016, Europe Patent No. EP2979666 2016 and China Patent No. CN103384505. The full list is available at https://www.wheatleyresearch.co.uk/blog/development-history

Please state any sources of funding for your research

São Paulo Research Foundation (FAPESP), Grant 2021/11129-0

Ethical Approval

Work on human beings that is submitted to *Medical Engineering & Physics* should comply with the principles laid down in the Declaration of Helsinki; Recommendations guiding physicians in biomedical research involving human subjects. Adopted by the 18th World Medical Assembly, Helsinki, Finland, June 1964, amended by the 29th World Medical Assembly, Tokyo, Japan, October 1975, the 35th World Medical Assembly, Venice, Italy, October 1983, and the 41st World Medical Assembly, Hong Kong, September 1989. You should include information as to whether the work has been approved by the appropriate ethical committees related to the institution(s) in which it was performed and that subjects gave informed consent to the work.

DOES YOUR STUDY INVOLVE HUMAN SUBJECTS? Please cross out whichever is not applicable.

Yes

x No

If your study involves human subjects you MUST have obtained ethical approval.
Please state whether Ethical Approval was given, by whom and the relevant Judgement's reference number

Nothing to declare.

DOES YOUR STUDY INVOLVE ANIMAL SUBJECTS? Please cross out whichever is not applicable.

Yes

x No

If your study involves animals you must declare that the work was carried out in accordance with your institution guidelines and, as appropriate, in accordance with the EU Directive 2010/63/EU**.** http://eur-lex.europa.eu/legal-content/EN/TXT/?uri=CELEX:32010L0063

Nothing to declare.

This information must also be inserted into your manuscript under the acknowledgements section prior to the References.

If you have no declaration to make please insert the following statements into your manuscript:

Competing interests: None declared

Funding: None

Ethical approval: Not required